Nuclear Magnetic Resonance Studies of Solidified H_2-D_2 Mixtures. II. Pulsed Techniques*

D. S. METZGER† AND J. R. GAINES‡
Department of Physics, Ohio State University, Columbus, Ohio
(Received 8 September 1965; revised manuscript received 24 March 1966)

Standard NMR pulse techniques are applied to the study of the H_2 resonance at 9.3 Mc/sec in solid nH_2-nD_2 mixtures at 4.2 and 1.1°K. At 4.2°K the Bloch decay for nH_2 exhibits an oscillatory behavior that resembles the beat structure in CaF_2 observed by Lowe and Norberg. This beat structure is not observed for nH_2 concentration below 0.25. At 1.1°K the splitting of the resonance line associated with the λ anomaly is seen as a distinct beat pattern of the Bloch decay. In addition to these Bloch decays, spin echoes that persist for times long compared to the time required for the Bloch decay to vanish are observed to follow a 90°-τ-β pulse sequence, τ being the time between pulses and β the rotation produced by the second pulse. The decay of the echoes as a function of 2τ is very nearly exponential and the associated time constant T_E, depends on the rotation β in such a way that T_E increases as β decreases. It is shown that as a result of the latter effect the echoes have maximum amplitude for $\beta=\frac{1}{2}\pi$ when τ is short but $\beta<\frac{1}{2}\pi$ when τ is long. The essential features of the Bloch decays and echoes are adequately accounted for by a single-particle model similar to the one used by Solomon to explain the multiple quadrupole echoes in KI. The Hamiltonian describing the energy-level spacing of a given ortho H_2 molecule (in the rotating frame) is taken as

$$\hat{H}'=-\Delta\omega h\hat{I}_z+\alpha h\hat{I}_z^2,$$

where the protons of the molecule are considered to be constituents of a particle with spin unity. The parameters $\Delta\omega$ and α represent, respectively, the static intermolecular line broadening and the secular intramolecular dipole-dipole interaction. The spin-lattice relaxation time T_1 was measured using repetitive $\pi/2$ pulses. It is shown that T_1 decreases as α increases.

I. INTRODUCTION

THE pulsed-magnetic-resonance data presented in this paper represent an extension of the steady-state results previously reported.[1] The anomalous saturation behavior of nH_2 and the interpretation given in Paper I in terms of the theory of Provotorov[2] indicated that direct measurements of T_2, the spin-spin relaxation time and T_1, the spin-lattice relaxation time would be of considerable interest. Furthermore it would be possible to obtain the shape of the steady-state line for H_1 (the magnitude of the rotating rf field) exactly equal to zero by taking the Fourier transform of the free induction decay observed in a pulsed experiment. Measurements of the relaxation times in solid H_2 had been reported previously by Bloom[3] but only down to the motional line shape transition near 10°K. In the vicinity of this temperature the linewidth increases rapidly from a fraction of a gauss to about six gauss giving rise to a short T_2, so short in fact that a considerable amount of the signal can be lost in the amplifier "blocking time" following an intense rf pulse.

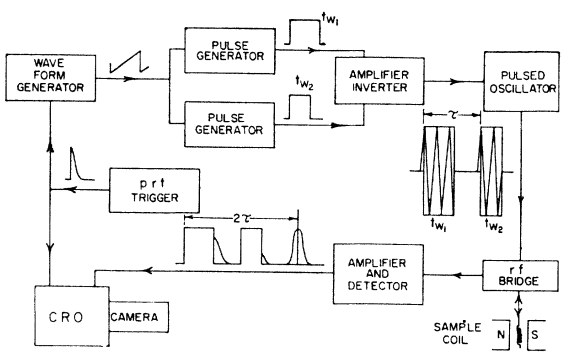

FIG. 1. Block diagram of the electronics.

Several interesting features were observed during the course of the above investigations, namely:

(i) The Bloch decay in nH_2 at 4.2°K is not a simple monotonically decreasing function of time describable by a Gaussian or exponential function but an oscillatory function similar to the Bloch decay in CaF_2 observed by Lowe and Norberg.[4]

(ii) Spin echoes were obtained in solid nH_2 and in H_2-D_2 mixtures at 4.2 and 1.1°K. These "solid echoes" persisted for times considerably longer than the time taken for the Bloch decay to go to zero. The pulse sequence used to obtain these echoes was not the usual 90°-τ-180° sequence but one employing a second pulse rotation of less than 90°.

A simple but physically realistic model is presented in this paper that combined with a mathematical development used by Solomon[5] (to explain the unusual sequence of "quadrupole echoes" he observed in KI) explains the essential features of (i) and (ii) and many features of other experiments on seemingly different solid sys-

* Work supported in part by a grant from the National Science Foundation and a contract with the U. S. Office of Naval Research.
† This work was submitted in partial fulfillment of the requirements for the Ph.D. degree at Ohio State University.
‡ Alfred P. Sloan Fellow.
[1] J. R. Gaines, E. M. de Castro, and J. G. Daunt, Phys. Rev. **140**, A319 (1965).
[2] B. N. Provotorov, Zh. Eksperim. i Teor. Fiz. **41**, 1582 (1961) [English transl.: Soviet Phys.—JETP **14**, 1126 (1962)].
[3] M. Bloom, Physica **23**, 767 (1957).
[4] I. J. Lowe and R. E. Norberg, Phys. Rev. **107**, 46 (1957).
[5] I. Solomon, Phys. Rev. **110**, 61 (1958).

tems[6–8] in which echoes have been observed. In fact the echoes (and their behavior) predicted by the model presented below can be considered as the more general case with the classical 90°-180° echoes as one particular limit.

II. EXPERIMENTAL ARRANGEMENT

Except for the electronics used for production, detection, and display of the NMR signal, the equipment used was the same as that described previously.[1] A block diagram of the electronics used is given in Fig. 1. The pulsed oscillator was produced by the Arenberg Ultrasonic Lab (Model PG650 C). Since the oscillations are produced by shock exciting an RLC circuit, there is no definite phase relationship between two successive radio-frequency pulses. This will be seen to be an important consideration in the following sections. A radio-frequency bridge similar to the one used by Lowe and Barnaal[9] satisfactorily protected the amplifier (L.E.L. IF 30 modified so that the center frequency was 9.3 Mc/sec) so that the blocking time was approximately 10 μsec. The gain of the amplifier was varied from 54 to 89 dB by adjusting the B^+ voltage while holding the bias voltage constant.

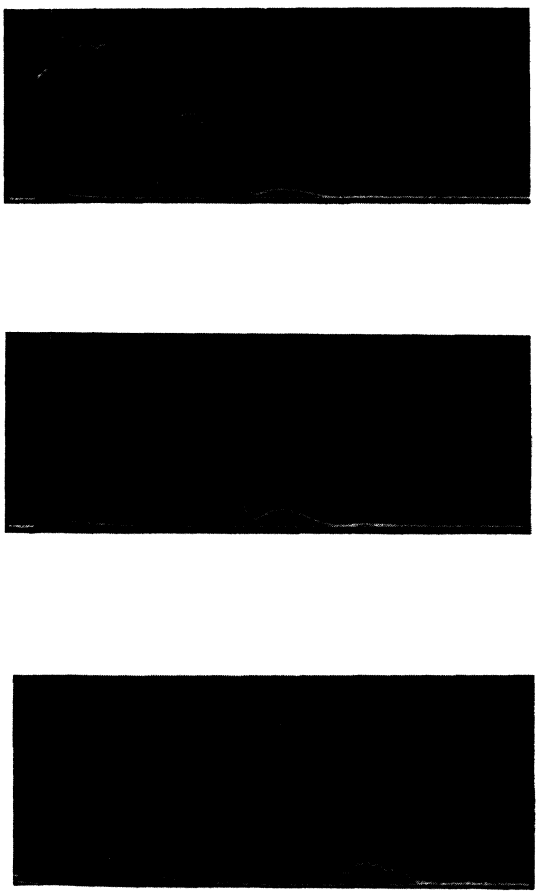

FIG. 2. Bloch decay for nH_2 at 4.2°K, $X=20$ μsec/division. (a) $Y=2$ V/division. (b) $Y=1$ V/division. (c) $Y=0.1$ V/division.

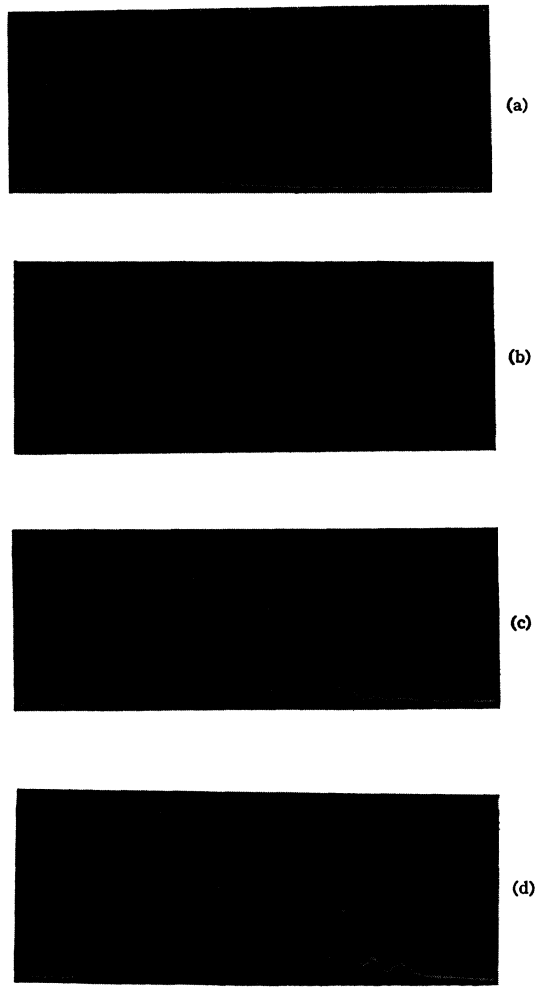

FIG. 3. Bloch decays for nH_2, $1.1°K \leq T < 4.2°K$. (a) $X=20$ μsec/division, $Y=1$ V/division, $T \approx 2°K$. (b) $X=20$ μsec/division, $Y=1$ V/division, $T \approx 1.5°K$. (c) $X=10$ μsec/division, $Y=1$ V/division, $T=1.1°K$. (d) $X=10$ μsec/division, $Y=0.5$ V/division, $T=1.1°K$.

III. RESULTS

The data to be presented in this paper were obtained from the Bloch decay or free induction decay (i.e., the signal following a 90° pulse), from measurements of the spin-lattice relaxation time (T_1), and from spin echoes stimulated by a two-pulse sequence $90°$-τ-β with τ being the time between pulses and β the rotation produced by the second pulse. A range of nH_2-nD_2 mixtures from 100% H_2 to 1% H_2 (all mixtures will be referred

[6] E. L. Hahn, Phys. Rev. **80**, 580 (1950).
[7] J. G. Powles and P. Mansfield, Phys. Letters **2**, 58 (1962); P. Mansfield, Phys. Rev. **137**, A961 (1965).
[8] J. G. Powles and J. H. Strange, Proc. Phys. Soc. (London) **82**, 6 (1963).
[9] I. J. Lowe and D. E. Barnaal, Rev. Sci. Instr. **34**, 143 (1963).

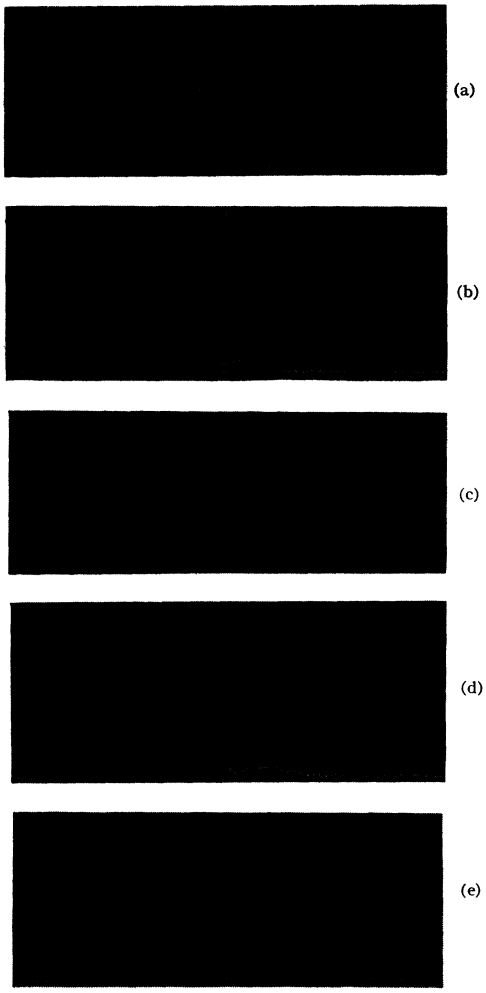

FIG. 4. Bloch decays for mixtures at 4.2°K, $Y=1$ V/division. (a) 75% H_2, $X=10$ μsec/division. (b) 75% H_2, $X=20$ μsec/division, gain×10.4 over (a). (c) 40% H_2, $X=10$ μsec/division. (d) 40% H_2, $X=20$ μsec/division, gain×22.4 over (c). (e) 25% H_2, $X=10$ μsec/division.

to in terms of their H_2 concentration) has been studied and pertinent examples of typical data will be given below.

(a) The Free Induction Decays

Photographs of oscilloscope traces are shown in the next few figures. The short trace in the left-hand portion of the photographs shows that the cathode-ray oscillograph (CRO) sweep starts a few microseconds before the initiation of the 90° pulse. Several of the photographs show in addition to the free induction decay, a second trace that illustrates the amplifier response when no signal is present (i.e., when the magnetic field is turned off). In Fig. 2, the Bloch decay in nH_2 at 4.2°K is given for different scope amplifications. The beat structure is very striking. Rotation of the sample produced no changes in the beat pattern for nH_2 as it did for CaF_2. Fourier transforms of the line shapes presented in Paper I also revealed this beat structure. This however is only an internal consistency check.

The beat structure in nH_2 is temperature-dependent as is evident in Fig. 3 which shows the beat pattern at about 2°K (slightly above the λ temperature of solid nH_2) in trace (a), the beat pattern momentarily after (a) in trace (b) just at the λ temperature, and traces (c) and (d) at 1.1°K well below the λ temperature. It should be noted that the beat frequency at 1.1°K is considerably higher than that at 4.2°K.

At 4.2°K beat patterns similar to those for nH_2 are observed for $x_{H_2'} \geqq 0.4$. For these patterns, however, the relative beat amplitude decreases with decreasing H_2 concentration while the null spacing increases slightly (see Fig. 4). The Bloch decay for the 25% mixture is a simple monotonically decreasing function of time as are the lower concentration mixtures not shown here.

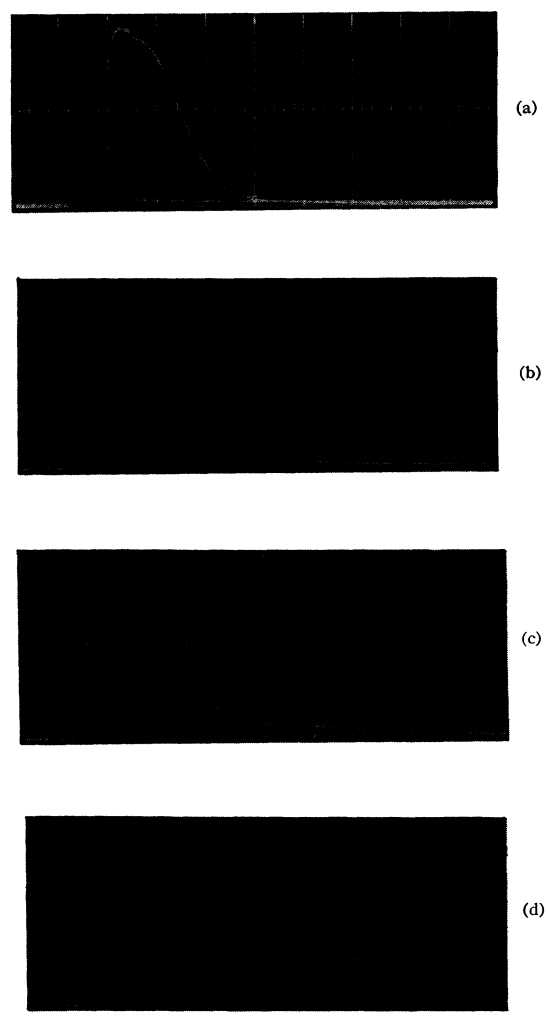

FIG. 5. Low-gain Bloch decays for mixtures at 1.1°K, $X=10$ μsec/division, $Y=1$ V/division. (a) 75% H_2. (b) 40% H_2. (c) 25% H_2. (d) 5% H_2.

TABLE I. T_1 for nH_2 from beats on Bloch decay at 1.1°K.

Beat	T_1(msec)
2nd	180
3rd	318
4th	300
5th	515
6th	495
7th	568

Figure 5 shows the Bloch decays for a few selected mixtures where the amplifier gain has been reduced so as to avoid saturation (of the amplifier) near the beginning of the Bloch decay. Further, the maximum observable signal near the beginning of the Bloch decay is adjusted to be about the same height, resulting in a sequence of signals effectively normalized to a single initial decay amplitude. Two features of these signals are immediately apparent: (1) As the H_2 concentration is decreased, a broad tail of the decay becomes more evident. (2) The widths of the narrow portion of the signals do not change appreciably. These two distinct portions of the Bloch decay at 1.1°K have different longitudinal relaxation times and these times differ from those obtained at 4.2°K.

(b) Longitudinal Relaxation (T_1)

The longitudinal relaxation times reported here were measured by two techniques: (1) A 180°-τ-90° sequence was used (curve A, Fig. 6) and (2) A 90°-τ-90°-τ-90°$\cdots$ sequence. The second sequence is quite useful for solids where $T_2 \ll T_1$ since one need only measure the signal height as a function of the pulse repetition rate. The values obtained differ by about 15% although each individual determination is accurate to about 2%. Unless otherwise stated, the values of T_1 reported here were obtained using the second method. The values of the

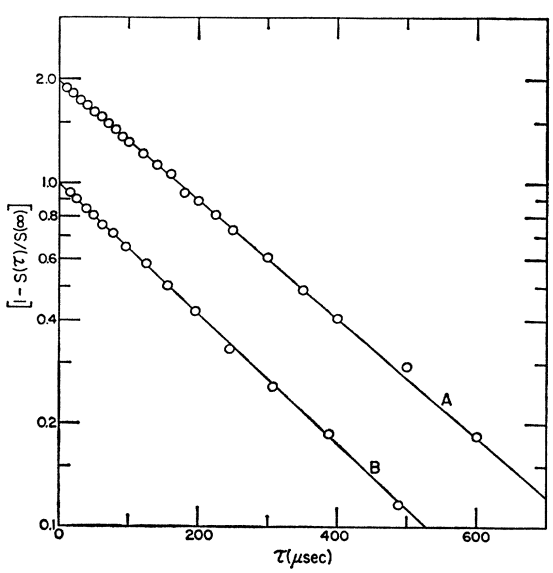

FIG. 6. T_1 data for nH_2 at 4.2°K, 9.3 Mc/sec. A: π-τ-$\pi/2$ pulse sequence, $T_1=252$ msec. B: Repetitive $\pi/2$ pulse sequence, $T_1=230$ msec.

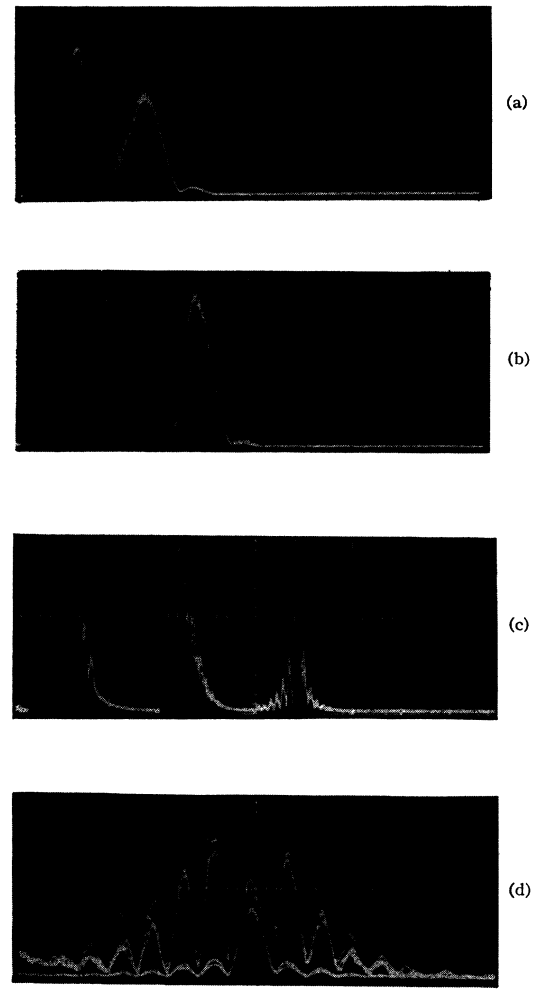

FIG. 7. Spin echoes for nH_2 at 4.2°K and 1.1°K. (a) $T=4.2$°K, $X=50$ μsec/division, $Y=1$ V/division. (b) $T=4.2$°K, $X=50$ μsec/division, $Y=0.1$ V/division. (c) $T=1.1$°K, $X=50$ μsec/division, $Y=0.2$ V/division. (d) $T=1.1$°K, expanded view of an echo (superposition of two photos). $X=10$ μsec/division, $Y=0.5$ V/division and 0.05 V/division.

TABLE II. T_1(msec) for nH_2-nD_2 mixtures.

	4.2°K		1.1°K	
%H_2	Beat	Bloch Decay	Narrow	Broad
100	275	215	See Table I	
75	295	265	95	105
50	270	305	95	145
45		235	125	135
40		240	135	130
35		280	180	...
25		250	140	160
10		235	195	315
5		275	230	325
1		610	...	1540

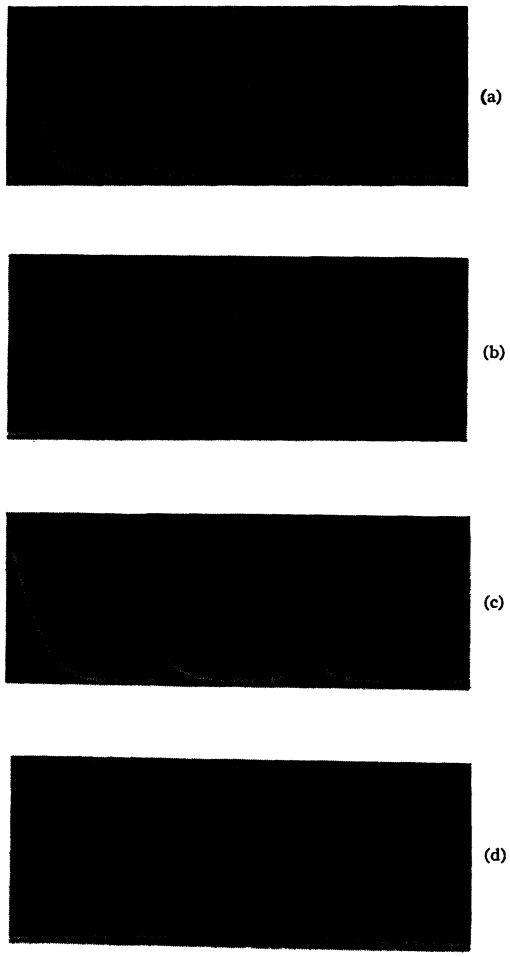

FIG. 8. Spin echoes for 5% mixture at 4.2°K and 1.1°K. (a) $T=4.2$°K, $X=100$ μsec/division, $Y=1$ V/division, $60°<\beta<90°$. (b) $T=4.2$°K, expanded view of echo, $X=20$ μsec/division. (c) $T=1.1$°K, $X=100$ μsec/division, $Y=1$ V/division, $60°<\beta<90°$. (d) $T=1.1$°K, expanded view of echo, $X=20$ μsec/division, $Y=1$ V/division.

longitudinal relaxation time for various beats on the free induction decay of nH_2 at 1.1°K are given in Table I.

The values of T_1 measured for various mixtures are collected in Table II. Where possible, T_1 was measured from the beat at 4.2°K as well as near the beginning of the Bloch decay. At 1.1°K, T_1 was measured for the broad and narrow portions of the Bloch decay at times near 45 μsec and 20 μsec, respectively, from the beginning of the trace.

(c) Spin Echoes

A two-pulse sequence, $90°$-τ-β, in general produces a spin echo at $t=2\tau$. Unlike classical spin echoes, which have maximum amplitude for $\beta=180°$, most of the echoes observed in H_2-D_2 mixtures exhibit maximum height for β less than 90°. The optimum value for β is between 40° and 60°; however, as will be noted for low H_2 concentration mixtures, certain echoes are maximized for $\beta=90°$ and $\beta=180°$.

(1) *General Description*

Figure 7 shows examples of echoes obtained from nH_2 at 4.2 and 1.1°K. In each case there is a beat structure on the tail of the echo that resembles the beats on the Bloch decay. This leads to the supposition, to be verified later, that in certain cases the echo may be an attenuated image of the Bloch decay. Also, the echo at 1.1°K is seen to be more narrow than those at 4.2°K. The occurrence of more narrow echoes at lower temperatures is typical of all the mixtures and is illustrated particularly well in Fig. 8.

The character of the echoes begins to change appreciably for the concentrations of 10% or lower. These changes are illustrated in Figs. 8 and 9 for the 5% and

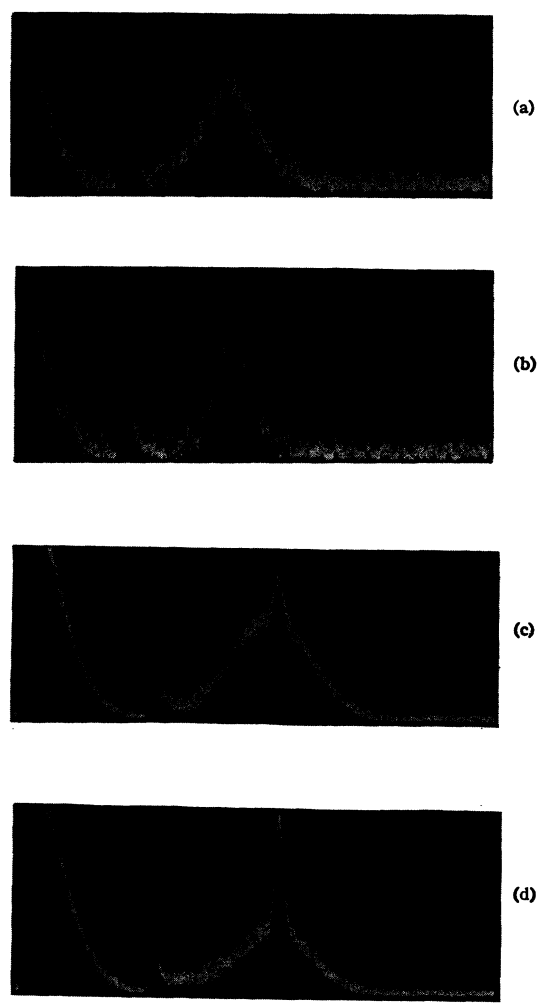

FIG. 9. Spin echoes for 1% mixture at 4.2°K and 1.1°K, $X=100$ μsec/division. (a) $T=4.2$°K, $\beta=180°$, $Y=0.5$ V/division. (b) $T=4.2$°K, $\beta=90°$, $Y=0.5$ V/division. (c) $T=1.1$°K, $\beta=180°$, $Y=1$ V/division. (d) $T=1.1$°K, $\beta=90°$, $Y=1$ V/division.

TABLE III. Echo full widths at half-maximum.

	$W_{1,1/2}$(μsec)	
%H_2	4.2°K	1.1°K
100	39	6
75	39	28
50	48	28
45	52	26
40	50	26
35	52	26
25	54	26
10	55	24
5	58	22
1	75	22
	140	180

1% mixtures, respectively. Figure 8 shows the echoes for the 5% mixture at 4.2 and 1.1°K. Both echoes are a maximum for β nearly equal to 90°; however, the 1.1°K echo exhibits a tail that is maximum for $90 \leq \beta \leq 180°$.

For the 1% mixture an interesting situation arises as is illustrated in Fig. 9. Two distinct echoes are observed at 4.2°K as well as at 1.1°K. At 4.2°K it is evident that a broader echo is produced for $\beta=180°$ than for $\beta=90°$. Likewise, at 1.1°K the broad part of the echo is a maximum for $\beta=180°$ and the narrow part peaks for $\beta=90°$. Actually the width of the broad decay for this concentration is determined by magnetic-field inhomogeneities. In Table III the echo full widths at half-maximum are given for each of the mixtures at 4.2 and 1.1°K. For the 1% mixture, the widths of both the broad and narrow echoes are given.

(2) *Echo Decays*

Since the echoes reported here persist for times long compared to the time required for the Bloch decay signal to disappear, it is possible to obtain a decay envelope for the echoes. Examples of echo decays are shown in Fig. 10 where multiple exposure photographs illustrate the change in echo amplitude as the time τ between the pulses is increased.

Semilog plots of the echo height versus 2τ show that the echo decay envelope can be represented by the function $h(2\tau)=h(0)\exp(-2\tau/T_E)$. It must be pointed out that in many cases (for instance the 10% mixture and lower concentrations) the decay data can be represented equally well by a Gaussian curve. Echo-decay-time constants for several of the mixtures are presented in Table IV. The values are accurate to about ±20% due to inability to determine β accurately and an observed dependence of T_E on β.

TABLE. IV. Echo-decay-time constants for $40° \leq \beta < 60°$.

	T_E(μsec)	
%H_2	4.2°K	1.1°K
100	25	60
75	40	60
50	50	80
45	105	...
40	90	110
35	137	140
25	150	240
10	150	390

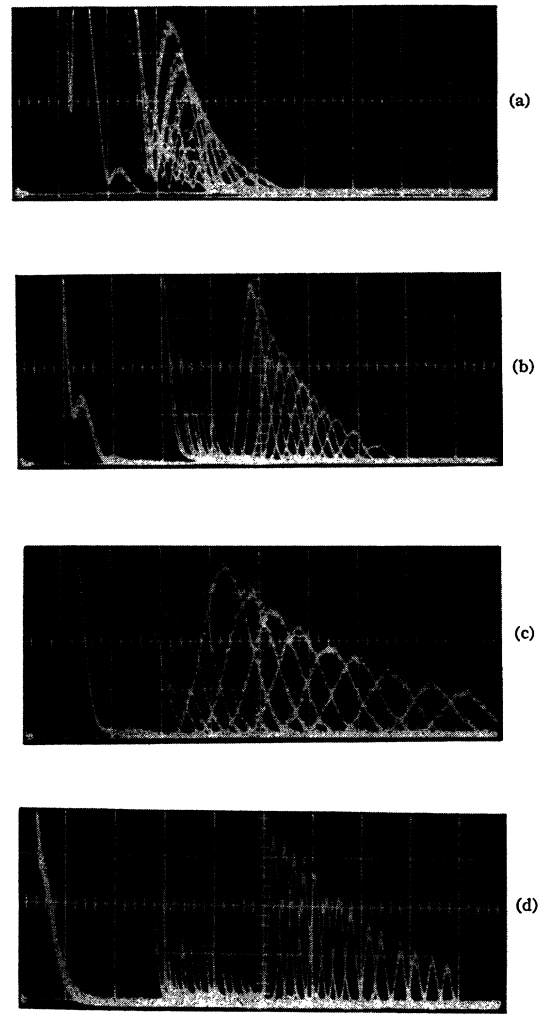

FIG. 10. Echo-decay envelopes at 4.2°K and 1.1°K, $Y=1$ V/division. (a) 75% H_2, $T=4.2$°K, $X=50$ μsec/division. (b) 75% H_2, $T=1.1$°K, $X=50$ μsec/division. (c) 25% H_2, $T=4.2$°K, $X=50$ μsec/division. (d) 25% H_2, $T=1.1$°K, $X=100$ μsec/division.

Examination of the echoes for times τ shorter than those displayed in Fig. 10 revealed the variations in echo height that are common in phase incoherent experiments and that the 90°-τ-90° sequence produced a potentially larger echo than the 90°-τ-β sequence where $\beta<90°$. This behavior is just the reverse of the behavior for larger τ suggesting that T_E may depend on β in such a manner that T_E decreases as β increases. Figure 11 illustrates two cases where the greater rotation β results in a shorter time constant T_E. The values of T_E obtained for various values of β are listed in Table V where the width of the second pulse is given rather than β.

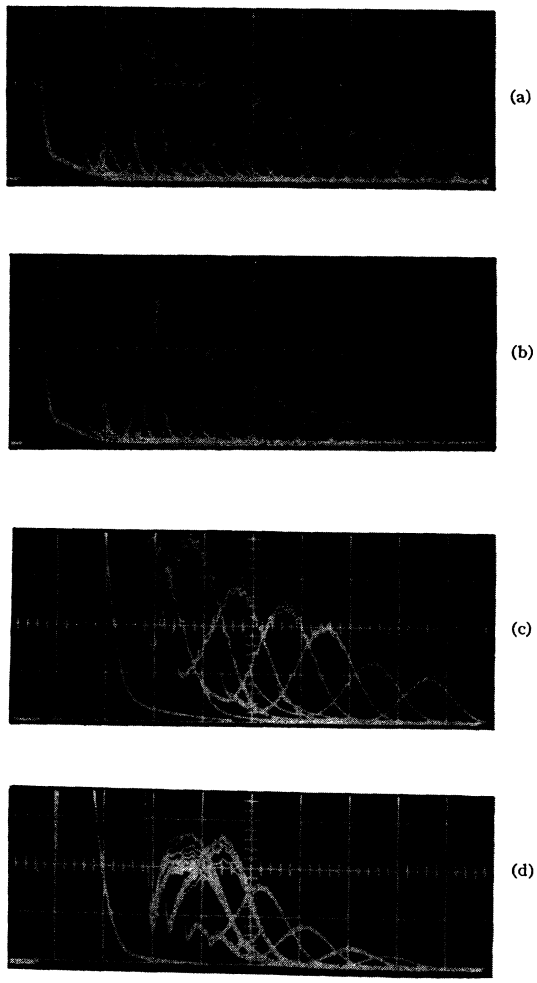

FIG. 11. Echo decays for different values of β at 1.1°K. (a) 25% H_2, $40° < \beta < 60°$, $X = 50$ μsec/division, $Y = 1$ V/division. (b) 25% H_2, $\beta = 90°$, $X = 50$ μsec/division, $Y = 1$ V/division. (c) 75% H_2, $40° < \beta < 60°$, $X = 20$ μsec/division, $Y = 0.5$ V/division. (d) 75% H_2, $\beta = 90°$, $X = 20$ μsec/division, $Y = 1$ V/division.

TABLE V. Comparison of T_E for different values of t_{w2}.

%H_2	T°K	t_{w2} μsec	T_E μsec
75	1.1	1.4	65±5
		2.4	30±5
45	4.2	1.8	104±4
		2.4	76±3
40	4.2	1.8	98±4
		2.0	72±2
	1.1	1.9	112±6
		2.4	68±10
25	1.1	1.8	205±15
		2.4	100±3
5	4.2	1.8	445±45
		2.1	376±35
1	4.2	2.4	500±50
		4.0	246±25

IV. THEORY

The calculation presented in this section will form the basis for interpreting the data, especially the spin echoes, presented in the previous section. A single-particle model similar to the one used by Solomon[5] is employed with the statistical variations of the parameters characterizing the model being taken into account by appropriate distribution functions. Because the Bloch decays and spin echoes we wish to describe take place on a time scale much shorter than T_1, spin-lattice relaxation is legitimately ignored. Although the calculation will deal explicitly with two spin-$\frac{1}{2}$ particles, it can be extended to more complex situations as shown in Appendix A.

(a) The Hamiltonian

The Hamiltonian of a pair of protons in an external magnetic field $H_0 = \omega_0/\gamma$ is written as

$$\hat{H} = -\hbar\omega_0(\hat{I}_{1z}+\hat{I}_{2z}) + \frac{\gamma^2\hbar^2}{r^3}\left[\hat{\mathbf{I}}_1\cdot\hat{\mathbf{I}}_2 - 3\frac{(\hat{\mathbf{I}}_1\cdot\mathbf{r})(\hat{\mathbf{I}}_2\cdot\mathbf{r})}{r^2}\right]. \quad (1)$$

When viewed from a frame of reference rotating about the applied field (z axis) with angular frequency ω, the Hamiltonian can be approximated by

$$\hat{H}' = -\hbar(\omega_0-\omega)(\hat{I}_{1z}+\hat{I}_{2z}) + \tfrac{1}{2}(\gamma^2\hbar^2/r^3) \times (1-3\cos^2\theta)[3\hat{I}_{1z}\hat{I}_{2z} - \hat{I}_1\cdot\hat{I}_2], \quad (2)$$

where the time-dependent terms in the dipolar interaction have been omitted leaving only the part that commutes with the Zeeman term. In terms of the usual triplet ($I=1$, $m=\pm1, 0$) states of the Zeeman Hamiltonian, one obtains for the energy levels of $\hat{H}'$

$$E_{-1} = \hbar(\omega_0-\omega) + (\gamma^2\hbar^2/4r^3)(1-3\cos^2\theta)$$
$$E_0 = -(\gamma^2\hbar^2/2r^3)(1-3\cos^2\theta)$$
$$E_{+1} = -\hbar(\omega_0-\omega) + (\gamma^2\hbar^2/4r^3)(1-3\cos^2\theta).$$

The same set of energy levels are obtained by considering the two spin-$\frac{1}{2}$ particles to be constituents of a spin-1 particle whose Hamiltonian is given by

$$\hat{H}_{\text{eq}}' = -\hbar(\Delta\omega)\hat{I}_z + \alpha\hbar\hat{I}_z^2 - \tfrac{2}{3}\alpha\hbar, \quad (3)$$

where $\Delta\omega = \omega_0 - \omega$ and $\alpha = (3/4)(\gamma^2\hbar/r^3)(1-3\cos^2\theta)$.

The singlet state ($I=0$, $m=0$) does not enter into the calculation, because the singlet and triplet states are not coupled through the Hamiltonian of Eq. (2). The coupling of a particle with its identical neighbor (e.g., the proton-proton coupling in the ortho-hydrogen molecule) is taken into account in the second term of Eq. (3); the first describes the static variations of the local field from molecule to molecule (i.e., between various spin-1 sites). The nonstatic variations in the local field effect spin-spin relaxation involving "spin-flip" terms that cannot be incorporated easily, but we will assume that in first order such terms will simply damp the transverse magnetization in time.

(b) Density Matrix in the Rotating Reference Frame and the Free Induction Decay

Before application of an rf pulse, the spin system is in thermal equilibrium and can be described by a density matrix given in the high-temperature approximation by

$$\hat{\rho}_0 \sim e^{-\gamma\hbar I_z H/kT} \cong 1-(\gamma\hbar\hat{I}_z H/kT).$$

The effect of an intense rf pulse, with amplitude H_1 larger compared to the interaction between the particles, is to rotate the equilibrium magnetization through the angle $\beta=\gamma H_1 t_w$ about an axis O_y, say, of the rotating frame. If we assume that the pulse width t_w is short compared to the spin-spin relaxation time, then the density matrix after a 90° pulse can be written at time zero as

$$\hat{\rho}_0(0) \cong 1-\gamma\hbar\hat{I}_x H/kT. \tag{4}$$

A pick-up coil in the XY plane of the stationary frame in the laboratory will see an induced signal proportional to the average value of the complex transverse magnetization ($\hat{I}_+=\hat{I}_x+i\hat{I}_y$). This signal may be calculated from

$$S(t)=\mathrm{Tr}[\hat{\rho}(t)\hat{I}_+], \tag{5}$$

where $\rho(t)$, the density matrix in the rotating frame, can be obtained from the initial value given in Eq. (4) by the usual time-evolution expression

$$\hat{\rho}(t)=\exp(-(i/\hbar)\hat{H}'t)\hat{\rho}(0)\exp((i/\hbar)\hat{H}'t), \tag{6}$$

with $\hat{H}'$ given by Eq. (3). Then the signal following a 90° pulse (Bloch decay) is obtained from

$$\begin{aligned} S(t)&=\mathrm{Tr}\{\exp[-i(\Delta\omega\hat{I}_z+\alpha\hat{I}_z^2)t]\hat{I}_x \\ &\qquad\times\exp[i(\Delta\omega\hat{I}_z+\alpha\hat{I}_z^2)t]\hat{I}_+\} \\ &=2\cos\alpha t\,\exp i\Delta\omega t. \end{aligned} \tag{7}$$

The result given in Eq. (7) must be integrated over appropriate distribution functions $f(\alpha)$ and $g(\Delta\omega)$ to yield the response of the entire sample to a 90° pulse. If these distribution functions are assumed to be even functions of α and $\Delta\omega$, respectively, the signal following a 90° pulse is proportional to

$$\begin{aligned} S(t)&=2\int f(\alpha)\cos\alpha t d\alpha\int g(\Delta\omega)\cos\Delta\omega t d\Delta\omega \\ &=2F(t)G(t), \end{aligned} \tag{8}$$

which is simply the product of the Fourier transforms of the two distribution functions.

(c) Spin Echoes

The effect on the density matrix produced by a second pulse of negligible width, applied τ seconds after the first, can be described by a unitary rotation operator $\hat{R}$ that operates on the spin coordinates in the rotating reference frame. The density matrix immediately after the second pulse, $\hat{\rho}'(\tau)$, is related to the value immediately before the pulse, $\hat{\rho}(\tau)$, by the expression

$$\hat{\rho}'(\tau)=\hat{R}\hat{\rho}(\tau)\hat{R}^{-1}.$$

The signal following the second pulse ($t>\tau$) is then obtained from

$$\begin{aligned} S(t)=\mathrm{Tr}\{&\exp[-(i/\hbar)\hat{H}'(t-\tau)]\hat{R}\exp[-(i/\hbar)\hat{H}'\tau]\hat{I}_x \\ &\times\exp[(i/\hbar)\hat{H}'\tau]\hat{R}^{-1}\exp[(i/\hbar)\hat{H}'(t-\tau)]\hat{I}_+\}. \end{aligned} \tag{9}$$

A straightforward calculation from Eq. (9), using for $\hat{H}'$ the Hamiltonian of Eq. (3), yields

$$\begin{aligned} S(t)=\sum_{m=0,1}\{&\sum_{m'=0,-1}\langle m|\hat{R}|m'+1\rangle \\ &\times\langle m'|\hat{R}^{-1}|m+1\rangle\exp[i\Delta\omega(t-2\tau)] \\ &\times\exp\{i\alpha[(2m+1)(t-\tau)-(2m'+1)\tau]\} \\ &+\sum_{m'=1,0}\langle m|\hat{R}|m'-1\rangle\langle m'|\hat{R}^{-1}|m+1\rangle\exp(i\Delta\omega t) \\ &\times\exp\{i\alpha[(2m+1)(t-\tau)+(2m'-1)\tau]\}\}. \end{aligned} \tag{10}$$

The matrix elements of the rotation operator $\hat{R}$ are the Wigner coefficients

$$\langle m|R|m'\rangle=D_{mm'}{}^1(\tilde{\alpha}\beta\gamma),$$

which are given in various reference works.[10] The particular elements of interest here are those for $\tilde{\alpha}=0$. The angle β then represents the rotation of the second pulse; while γ represents some arbitrary phase angle between the axis of rotation for the first pulse (0_y axis) and that for the second pulse. The angle γ is included to correspond to the phase-incoherent apparatus used in the present study. The operations described by these elements are, in order: (1) a rotation of the spin eigenstates through the arbitrary angle γ about the 0_z axis and (2) rotation about the 0_y axis through the angle β.

After integration over the distribution functions for α and $\Delta\omega$, the signal following the second pulse can be put in the form

$$S(t)=A(t)e^{-i\gamma}+B(t)e^{i\gamma}, \tag{11}$$

with $A(t)=G(t-2\tau)[\cos\beta(1-\cos\beta)F(t)-\sin^2\beta F(t-2\tau)]$ and $B(t)=G(t)[\cos\beta(1+\cos\beta)F(t)+\sin^2\beta F(t-2\tau)]$, where $F(t)$ and $G(t)$ are the Fourier transforms of the distribution functions as indicated in Eq. (8).

The actual signal observed in the NMR experiment is proportional to the modulus of Eq. (11). The terms that are responsible for spin echoes contain factors that are functions of $t-2\tau$ such that at $t=2\tau$ the term in question becomes independent of α or $\Delta\omega$ or both. Factors that do not have this time dependence are damped since $|F(t)|\leq F(0)=1$ and similarly for $G(t)$.

It should be noted that by relaxing the assumption that the first pulse produces only a rigid rotation of the spins through 90°, one obtains terms in the density

[10] M. E. Rose, *Elementary Theory of Angular Momentum* (John Wiley & Sons, Inc., New York, 1957).

matrix that permit transitions such that $\Delta m=\pm 2$. These transitions lead to an echo term at $t=3\tau$ that is damped by $G(t)$, the derivative of $F(t-\tau)$ with respect to time, and the ratio of the strength of the particle-particle interaction to H_1. No such echo has been observed.

(d) Special Cases

The following special cases of the above calculation are considered because they illustrate simple applications of the theory and throw considerable light on the echoes observed by Powles and Mansfield[7] for the protons in gypsum ($Ca_2SO_4\cdot 2H_2O$).

(i) *No Attenuation Due to the α Distribution*

$$F(t)=F(0)=1$$

In this case the signal is

$$S(t)=-2\sin^2(\beta/2)e^{-i\gamma}G(t-2\tau)+2\cos^2(\beta/2)e^{i\gamma}G(t)\,. \quad (12)$$

This result is identical to the classical-vector-model expression for the signal following the second pulse, predicting an echo at $t=2\tau$ that has a maximum height for $\beta=180°$ (see Appendix B). The second term in Eq. (12) does not contribute to the echo but will beat[11] against the echo (if no definite phase relationship, γ, exists between the two pulses) until attenuation due to the distribution in $\Delta\omega$ damps the term out.

(ii) *No Attenuation Due to the $\Delta\omega$ Distribution*

$$G(t)=G(0)=1\,.$$

In this case the signal takes the form

$$S(t)=2\cos\gamma\cos\beta F(t)+2i[\sin\gamma\sin^2\beta F(t-2\tau)+\cos\gamma\cos^2\beta F(t)]\,. \quad (13)$$

This is the spin-1 counterpart of the problem solved by Solomon.[5] No echo is predicted by Eq. (13) for the case where both rotations take place about the same axis (i.e., $\gamma=0$), a condition usually satisfied in an experiment using coherent pulses. If, however, a phase shift of 90° is introduced between the two pulses (i.e., $\gamma=\frac{1}{2}\pi$), one has the experimental conditions used by Powles and Mansfield[7]; and one has an echo.

(iii) *Relation to the Results of Powles and Mansfield*

Looking more closely at the form of the signal for the case where $\gamma=\pi/2$, we see

$$S(t)=i\{\sin^2\beta F(t-2\tau)[G(t-2\tau)+G(t)]+\cos\beta(1+\cos\beta)F(t)G(t)-\cos\beta(1-\cos\beta)F(t)G(t-2\tau)\}\,. \quad (14)$$

[11] Two terms are said to beat one against the other when their sum is dependent on their relative phases. This is observed experimentally in a phase incoherent experiment as a random variation in the amplitude of two additive signals upon repeating the pulse sequence that produces the signals.

The term that is independent of both α and $\Delta\omega$ at $t=2\tau$ gives a maximum echo for $\beta=90°$ in agreement with the results of Powles and Mansfield.

These authors also observe that a 90°-τ-180° pulse sequence gives essentially no echo independent of the phase shift and that a 90°-τ-90° sequence with no phase shift produces no echo. The latter observation is consistent with Eq. (13) (i.e., little attenuation due to the $\Delta\omega$ distribution); the former observation is expected for a second pulse rotation of 180° where the signal,

$$S(t)=-2F(t)G(t-2\tau)e^{-i\gamma}\,,$$

will be small and independent of γ if there is considerable attenuation due to the α distribution.

Thus the experimental results of Powles and Mansfield can be explained by this model if one assumes a narrow distribution for $\Delta\omega$ and a broad distribution for α. Both assumptions are physically reasonable for gypsum where, as shown by Pake,[12] the widths of the $\Delta\omega$ and α distributions are about 3 G (for the powder) and 10 G, respectively.

(e) Phase Incoherence and Echo Attenuation

Some final remarks are appropriate regarding the experiment in which no definite phase relationship exists between the two pulses, and the effects of F and G on the echo amplitude. If, as before, we call T_E the time constant measured from the echo decay envelope, then we predict that in general T_E will be a function of β, the rotation angle of the second pulse. For example, the signals at $t=2\tau$ for three specific values of $\beta(\beta=60°, 90°, 180°)$ are as follows:

$$\begin{aligned} S_{60°}(2\tau)&=\tfrac{1}{4}e^{-i\gamma}[F(2\tau)-3]+\tfrac{3}{4}e^{9\gamma}[F(2\tau)+1]G(2\tau)\,,\\ S_{90°}(2\tau)&=-e^{-i\gamma}+e^{i\gamma}G(2\tau)\,,\\ S_{180°}(2\tau)&=-2e^{-i\gamma}F(2\tau)\,. \end{aligned} \quad (15)$$

It is clear that F or G or both will affect the echo amplitude apart from the attenuation due to spin-flip terms not included in this calculation. The 180° decay envelope will yield information regarding the attenuation due to the α distribution whereas the 90° envelope is attenuated by the $\Delta\omega$ distribution in one term and by spin-flip processes only in the other. The 60° envelope is more complicated, the four terms being attenuated by F, G, FG, and spin-flip processes.

In a phase incoherent experiment the magnitude of the beating between the two terms that are out of phase [in general the A and B terms of Eq. (11)] depends on the relative magnitude of the two terms. When $F(2\tau)=G(2\tau)=0$, attenuation of the echo is due entirely to nonstatic (spin-flip) contributions and no beating occurs.

V. DISCUSSION

A particularly interesting effect observed in connection with the spin echoes for all the concentrations at

[12] G. E. Pake, J. Chem. Phys. 16, 327 (1948).

both temperatures is the dependence of T_E, the echo decay time, on β, the rotation produced by the second pulse. When the time between pulses τ is long, the dephasing due to the α and $\Delta\omega$ distributions is almost complete implying $F(2\tau)=G(2\tau)=0$. In this case, the signal is simply proportional to $S(2\tau)=\sin^2\beta$ and has its maximum value for $\beta=90°$. An exponential decay of the signal can be introduced by writing $S(2\tau)=\sin^2\beta \times\exp(-2\tau/T_E)$ where, however, the decay time constant depends on β in such a way that $T_E\beta\approx c$ is approximately true. Then the value of β that produces a maximum echo is obtained from $\tan\beta_{\max}=c/\tau$. Thus when τ is small compared to c (which is of order T_E), $\beta_{\max}$ is approximately $\pi/2$, but when τ is comparable to T_E (and c) as in most of the echo decay data, $\beta_{\max}$ is approximately $\pi/4$.

The dependence of T_E on β is much more noticeable in the low H_2 concentration mixtures, since in the high concentration mixtures the value of c/τ does not vary appreciably from unity over the range of τ available (i.e., $\tau\geq T_2\approx T_E$). Thus since the tangent function varies slowly when its argument is near unity, only a very slight dependence of T_E on β can be observed in the higher concentration mixtures. When the β dependence of T_E is taken into account, the agreement of the experimental spin echo data with the theory of Sec. IV is excellent.

(a) Pure nH_2

The oscillatory Bloch decay of nH_2 at 4.2°K (see Fig. 2) was similar to the decay observed in CaF_2[4] which could be described by the analytic function[13]

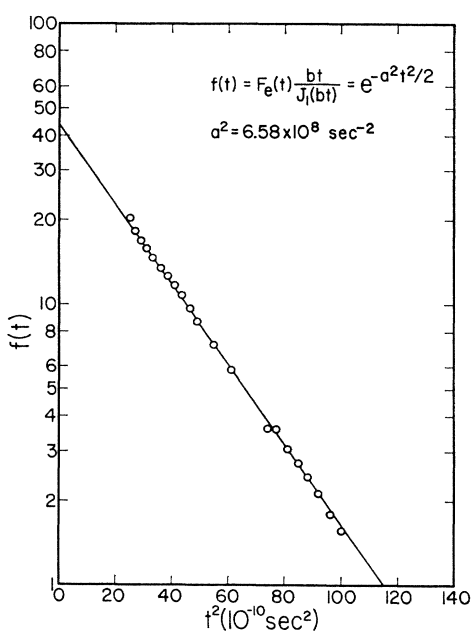

FIG. 12. Semilog plot of $F_{\text{expt}}(t)(bt/J_1(bt))$ versus t^2.

[13] A. Abragam, *The Principles of Nuclear Magnetism* (Oxford University Press, New York, 1961), Chap. 4.

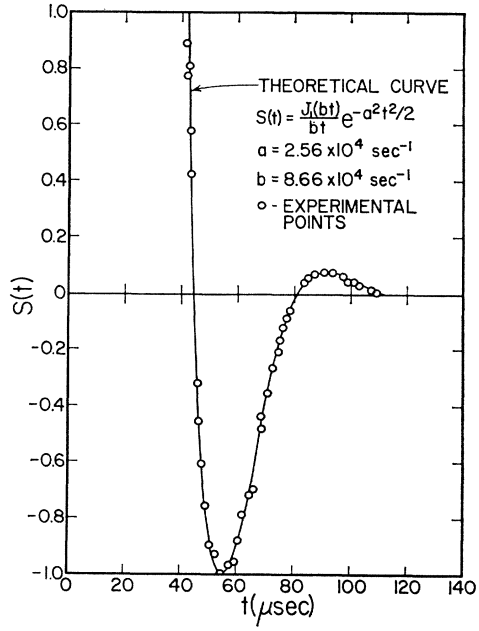

FIG. 13. Fit of line-shape function to experimental data.

$S(t)=\exp(-a^2t^2/2)(\sin bt)/bt$. However, in nH_2 the nulls of the Bloch decay are not evenly spaced; hence the function $J_1(bt)/bt$ appears more suitable than $\sin bt/bt$. In Fig. 12 the experimental data points have been multiplied by $[J_1(bt)/bt]^{-1}$ (where b was determined from the nulls of the Bloch decay) and plotted as a function of t^2. This permits determination of the parameter a. In Fig. 13 the experimental points are plotted along with the analytic fit; the agreement is excellent. It is usually more convenient to work analytically with the function containing $\sin bt/bt$ even though the fit it not as good.

The cw line shape corresponding to the function $\exp(-a^2t^2/2)(\sin bt)/bt$ is a superposition of Gaussian curves of rms half-width a under a rectangular envelope of width $2b$; the Bessel function implies a superposition of Gaussians under a semicircle of radius b. The Fourier transforms and moments corresponding to these two curves are given in Appendix C. The parameters determined from the pulse data (fitted to both functions) are given in Table VI and compared to the recent experimental data of Dickson and Meyer[14] (D and M). As can be seen from the table, the cw data of Dickson and Meyer give higher values of the second and fourth moments (M_2 and M_4, respectively) than the pulse data; however, the ratios of the various parameters are in good agreement. Further, it is important to note that the values of M_2, particularly for the pulse data, are in good agreement with the value of 63.1 (kc/sec)^2 calculated by Reif and Purcell[15] using the Van Vleck method.

The line-shape function implied by the oscillatory Bloch decay suggests a superposition of unresolved

[14] S. A. Dickson and H. Meyer, Phys. Rev. **138**, A1293 (1596).
[15] F. Reif and E. M. Purcell, Phys. Rev. **91**, 631 (1953).

TABLE VI. Parameters of the cw line shape at 4.2°K.

	a kc/sec	b kc/sec	ΔH[a] kc/sec	M_2 (kc/sec)^2	$M_4\times10^{-4}$ (kc/sec)^4	$\frac{\Delta H}{M_2^{1/2}}$	$\frac{M_4}{(M_2)^2}$
Rectangle	4.08	11.6	23.2±0.1	62±7	0.92±0.2	2.98±0.15	2.40±0.04
Semicircle	4.08	13.8	<27.6±0.1	64±7	1.03±0.2	<3.46±0.15	2.52±0.08
D and M			25.6±0.8	75±1	1.35	2.95±0.15	2.39

[a] ΔH is defined to be the linewidth as measured from the maximum and minimum on the derivative curve.

doublets that one is tempted to attribute to the "crystalline field splitting." The term crystalline field splitting refers to the perturbation of the Zeeman levels as a result of the intramolecular dipole-dipole interaction in accord with the discussion of Sec. IV. As described by Reif and Purcell[15] the magnitude of this effect depends on the degree to which the rotational degeneracy of the ortho-molecules is removed by internal electric fields. However, the agreement of the experimental and calculated second moments indicates that the line shape is primarily due to intermolecular dipole interactions. This suggestion is supported by the relatively short time persistence of the spin echoes and the similarity of the Bloch decay for nH$_2$ to that for CaF$_2$. Thus at 4.2°K we consider the line shape to be governed by intermolecular interactions, the crystalline field splitting contribution being small and undetermined. The situation is much different at 1.1°K.

The absorption line shape observed near 1.1°K by Reif and Purcell[15] can be described roughly in the following way. There exists a central Gaussian peak of rms half-width a_0 flanked on each side by a Gaussian peak of rms half-width a_1. The side peaks are centered at frequencies $\pm\delta/2$ from the central peak. The Bloch decay that is represented by the Fourier transform of such a line configuration is

$$S(t)=h_0\exp(-a_0^2t^2/2)+2h_1\exp(-a_1^2t^2/2)\cos\delta/2t,$$

where h_0 and h_1 are the heights of the central and side peaks, respectively. The central line merely causes the second term to oscillate about a decreasing base line rather than a horizontal line. From the observation (see Fig. 3) that the oscillations disappear at about the same time that the base line decays to zero, it is estimated that the central and side peaks have about the same half-width. This width is estimated from the decay of the base line to be about 14 kc/sec. Further, the splitting δ is calculated from the beat frequency to be 167±3 kc/sec in excellent agreement with Reif and Purcell.

The Bloch decay at 4.2°K is indicative of a narrow α distribution while that at 1.1°K shows an α distribution that is broad and double-peaked. The transition from the narrow to the broad α distribution is seen in the sequence of photographs in Figs. 2 and 3. The longer echo decay time constant T_E at 1.1°K is associated with the relative improbability of spin-flip processes that conserve Zeeman energy. Explanation of the fact that the relaxation time T_E remains much smaller than the spin-lattice relaxation time can be found in the work of Bloembergen, Shapiro, Pershan, and Artman.[16] The large residual central line that results from molecules in regions of high field symmetry may provide a medium for spin-spin relaxation in this sense.

The spin-lattice relaxation times reported here are more accurate than the ones obtained from steady-state saturation experiments (such as reported in Paper I) due to the difficulty in obtaining low enough modulation frequencies. The T_1's obtained in steady-state experiments can be brought into agreement with our pulse measurements by applying the modulation corrections described by Portis[17] for an inhomogeneously broadened line. The fact that different portions of the free induction decay relax toward the lattice temperature with different rates (see Tables I and II) is not understood. Sugawara[18] assumed that T_1 depended upon the location of a given isochromat relative to the center of the line in an effort to explain the anomalous saturation data in nH$_2$. Our observed dependence, however, does not agree with his assumption that $T_1\propto(\Delta\omega)^2$. Most features of the spin-lattice relaxation can be accounted for by postulating that the dominant interaction is of the quadrupole-quadrupole type that is governed by the parameter α and is, therefore, very sensitive to the rotational motion.

(b) nH$_2$-nD$_2$ Mixtures

In general the width of the resonance line will contain contributions from both intermolecular interactions and the crystalline field splitting. Although the latter effect is very small in nH$_2$ at 4.2°K, the widths of the spectral distributions in the mixtures change as a function of both concentration and temperature in a manner indicative of appreciable crystalline field effects.

The width of the spectral lines for the various mixtures were obtained from the inverse echo widths at half maximum, and the data so obtained are shown in Table VII. The apparent validity of this procedure for

[16] N. Bloembergen, S. Shapiro, P. S. Pershan, and J. O. Artman, Phys. Rev. **114**, 445 (1959).
[17] A. M. Portis, Phys. Rev. **91**, 1071 (1953).
[18] T. Sugawara, Sci. Rept. Res. Inst. Tohoku Univ. Ser. A **8**, 95 (1956).

widely different line shapes is illustrated for the particular case of nH_2 where the widths in Table VII agree very well with those obtained earlier by other methods.

The behavior of the linewidth or root second moment as a function of concentration in the mixtures can be calculated readily considering only intermolecular interactions. This has been cone in Paper I and yields,

$$M_2^{1/2}(x)=M_2^{1/2}(x=1)[x+k(1+x)]^{1/2},$$

where x is the nH_2 concentration, and the value of k averaged over all D_2 spin states is 0.021.

At 4.2°K the linewidths obviously do not decrease as rapidly as predicted by the above equation. For example, according to the calculations, the width for the lowest concentration mixture should be 17% of the value obtained for nH_2 rather than the observed 52%. The discrepancy is attributed to the crystalline field splitting. Perhaps it should be pointed out that the data in Table VII are weighted toward the broad tails of the spectral distribution whereas the similar data in Paper I are weighted toward the central component of the line shape.

At 1.1°K the effect is even more striking as the linewidths show a slight increase as the concentration is decreased. There is, of course, the exception for nH_2 where the molecular rotation is quenched. This behavior is very interesting, because one might expect the crystalline field splitting to decrease as the number of spherically symmetric molecules (ortho D_2) in the mixture is increased. However, it appears that the primary effect of the increased number of ortho-D_2 molecules is to increase the number of ortho-H_2 molecules that are relatively unperturbed by crystalline fields and contribute to the broad tails of the echoes (see Figs. 8 and 9). As might be expected for these isolated spins, the broad echo tails appear to behave classically with regard to the echo phenomenon. That the crystalline field effect is not completely washed out at the low concentrations is attributed to the fact that many ortho-hydrogen molecules may find themselves at sites of strong crystalline fields even at low concentration. For example, for any lattice site the most probable number of nearest neighbors having the rotational quantum number $J=1$ (ortho H_2 or para D_2) is four in the case of the 1% mixture.

TABLE VII. Linewidths for the mixtures as obtained from the echo widths at half maximum.

	ΔH(kc/sec)	
%H_2	4.2°K	1.1°K
100	25.6±0.6	167±5
75	25.6±0.6	35.8±1.0
50	20.8±0.5	35.8±1.0
45	19.2±0.3	38.4±1.6
40	20.0±0.4	38.4±1.6
35	19.2±0.3	38.4±1.6
25	18.5±0.4	38.4±1.6
10	18.2±0.2	41.6±1.6
5	17.2±0.3	45.4±2.0
1	13.3±0.3	45.4±2.0

VI. SUMMARY

The pulsed nuclear magnetic resonance data on nH_2 and nH_2-nD_2 mixtures lead to a clear interpretation of the resonance line shapes obtained in the solid hydrogens. The magnetic sublevels are split by unequal amounts due to the intramolecular interaction between the protons in a given ortho molecule. At 4.2°K the splitting of the sublevels is small compared to the perturbation by intermolecular interactions that result in both homogeneous and inhomogeneous broadening of the line. As a result the cross relaxation time represented by the echo decay time constant is comparable to the time required for the Bloch decay to vanish. At the lower temperatures (below 2°K) for nH_2, the crystalline field splitting becomes dominant. The cross relaxation time is longer in this case because the splitting represented by the α distribution is larger than that represented by the $\Delta\omega$ distribution as is apparent from the nearly resolved lines. The mixtures provide intermediate examples of unresolved doublets where the crystalline field effect is nevertheless appreciable.

The single-particle model used in Sec. IV is similar to the model used to derive the Curie-Weiss law in that the many-particle spin-spin interactions are replaced by a term containing the interaction of a single spin with an effective field. The crucial term is the one proportional to $\hat{I}_z^2$ since it is this term that leads to such distinctive features as : the echoes need not resemble the Bloch decay, the optimum rotation angle for the second pulse is spin-dependent, and pulse separations can be used that are greater than the time required for the Bloch decay to vanish. This particularly simple model explains many of the features (in particular the importance of an rf phase shift between pulses in some instances and not in others) observed in previous experiments concerned with echoes in solids. The experimental echo data in H_2-D_2 mixtures are in good agreement with the predictions of the theoretical model provided one takes into account the observed dependence of the echo decay time constant on the rotation produced by the second pulse.

ACKNOWLEDGMENTS

We wish to acknowledge Dr. E. M. de Castro who participated in our early experiments using pulsed techniques, Professor J. G. Daunt for his continuing interest in our work, Professor Jan Korringa for several interesting discussions regarding relaxation in solids, Dr. E. R. Hunt of Duke University for pointing out the contributions of Powles and co-workers, and Dr. W. E. Jones of Battelle Memorial Institute for many informative discussions regarding our data.

APPENDIX A: EXTENSION OF THEORY TO OTHER SYSTEMS

The model calculation presented in Sec. IV can be extended to other, more complicated systems. The only requisite for the formalism of Sec. IV to apply is that the system be described by a Hamiltonian of the form

$$\hat{H}'=\Delta\omega\hbar\hat{I}_z+\alpha\hbar\hat{I}_z^2+\text{constant}. \tag{A1}$$

Two such systems that may be of interest are (1) three spin-$\frac{1}{2}$ particles (protons) located at the vertices of an equilateral triangle and (2) the deuterium molecule.

Three Spin-$\frac{1}{2}$ Particles

The dipolar Hamiltonian for three spin-$\frac{1}{2}$ particles at the vertices of an equilateral triangle is

$$\hat{H}=\sum_{j<k}\frac{\hbar^2\gamma^2}{r^3}\left\{\mathbf{I}_j\cdot\mathbf{I}_k-\frac{3(\mathbf{I}_j\cdot\mathbf{r}_{jk})(\hat{\mathbf{I}}_k\cdot\mathbf{r}_{jk})}{r^2}\right\}. \tag{A2}$$

Keeping only the secular terms, we have in the rotating frame

$$\begin{aligned}\hat{H}'=&-\hbar(\omega_0-\omega)(\hat{I}_{1z}+\hat{I}_{2z}+\hat{I}_{3z})\\&+(\hbar^2\gamma^2/r^3)\sum_{j<k}(1-3\cos^2\theta_{jk})\\&\times[I_{jz}\cdot I_{kz}-\tfrac{1}{4}(I_{+j}I_{-k}+I_{-j}I_{+k})],\end{aligned} \tag{A3}$$

where θ_{jk} is the angle between $\mathbf{r}_{jk}$ and the external magnetic field.

The eigenstates for the three-particle system can be written as a group of four spin-$\frac{3}{2}$ states and two groups of two spin-$\frac{1}{2}$ states. Only the quartet of states,

$$\begin{aligned}&(+++),\\&(1/\sqrt{3})[(++-)+(+-+)+(-++)],\\&(1/\sqrt{3})[(--+)+(-+-)+(+--)],\\&(---)\end{aligned}$$

is of interest here. The splitting of the spin-$\frac{1}{2}$ states is unaffected by the dipolar Hamiltonian and there is no coupling between the three groups of states. Thus, the doublet states give rise to classical behavior as regards the spin echoes.

The energy levels associated with the four spin-$\frac{3}{2}$ states are:

$$\begin{aligned}E_{-3/2}&=\tfrac{3}{2}\hbar(\omega_0-\omega)+\tfrac{3}{4}(\gamma^2\hbar^2/r^3)(1-\cos^2\theta),\\E_{-1/2}&=\tfrac{1}{2}\hbar(\omega_0-\omega)+\tfrac{1}{4}(\gamma^2\hbar^2/r^3)(1-\cos^2\theta),\\E_{1/2}&=-\tfrac{1}{2}\hbar(\omega_0-\omega)+\tfrac{1}{4}(\gamma^2\hbar^2/r^3)(1-\cos^2\theta),\\E_{3/2}&=-\tfrac{3}{2}\hbar(\omega_0-\omega)+\tfrac{3}{4}(\gamma^2\hbar^2/r^3)(1-\cos^2\theta),\end{aligned}$$

where $\cos^2\theta=\cos^2\theta_{12}+\cos^2\theta_{13}+\cos^2\theta_{23}$. These energy levels can be generated by the Hamiltonian in Eq. (A1) with

$$\alpha=(\gamma^2\hbar/4r^3)(1-\cos^2\theta)$$

and

$$\text{const}=\tfrac{3}{4}\alpha\hbar.$$

Deuterium Molecule

For deuterium there are five symmetric spin-2 states and three antisymmetric spin-1 states to be considered. Also, deuterium differs from hydrogen in that there exists a quadrupolar coupling between the nuclei in addition to the dipolar coupling.

The main problem in this case is separating the dipolar and quadrupolar contributions to the Zeeman-level splitting. However, if one assumes that the quadrupole coupling dominates, one has for the quadrupole coupling

$$\hat{H}_Q=\frac{eQV_{zz}}{4I(2I-1)}[3I_z^2-I(I+1)] \tag{A4}$$

keeping only the secular terms. In Eq. (A4), V_{zz} represents the electric field gradient in the direction of the external field, and Q the nuclear quadrupole moment. Thus, the Hamiltonian corresponding to (A1) in this case is

$$\hat{H}'=\Delta\omega\hbar I_z+\alpha\hbar I_z^2+\text{const.}$$

with

$$\alpha\hbar=3eQV_{zz}/4I(2I-1).$$

APPENDIX B: QUANTUM-MECHANICAL DERIVATION OF CLASSICAL SPIN ECHOES

The distinction between classical spin echoes and the echoes discussed in Sec. IV is that the optimum rotation angle β of the second pulse is independent of nuclear spin for the classical echoes. The relation Eq. (12) is derived below on a quantum-mechanical basis similar to that used in Sec. IV.

In the rotating frame the Hamiltonian is

$$\hat{H}'=-\hbar\Delta\omega\hat{I}_z. \tag{B1}$$

Following Eq. (9) the signal after a 90°-τ-β sequence can be written as

$$\begin{aligned}S(t)=\mathrm{Tr}\{&\exp[-(i/\hbar)\hat{H}'(t-\tau)]\hat{R}\exp[-(i/\hbar)\hat{H}'\tau]I_x\\&\times\exp[(i/\hbar)\hat{H}'\tau]\hat{R}^{-1}\exp[(i/\hbar)\hat{H}'(t-\tau)]I_+\}.\end{aligned} \tag{B2}$$

Because of the simple form of $\hat{H}'$, one can conveniently take the rotation operator in the form

$$R(0,\beta,\gamma)=\exp(-i\beta\hat{I}_y)\exp(-i\gamma\hat{I}_z)$$

where the angles β and γ have the same meaning as in Sec. IV. Then using the fact that the trace is invariant to cyclic permutation, one has

$$\begin{aligned}S(t)=\mathrm{Tr}\{&e^{-i\beta\hat{I}_y}e^{-i(\varphi_0+\gamma)\hat{I}_z}\hat{I}_xe^{i(\varphi_0+\gamma)\hat{I}_z}e^{i\beta\hat{I}_y}\\&\times e^{i(\varphi-\varphi_0)\hat{I}_z}\hat{I}_+e^{-i(\varphi-\varphi_0)\hat{I}_z}\},\end{aligned} \tag{B3}$$

where $\varphi=\Delta\omega t$ and $\varphi_0=\Delta\omega\tau$. Then using the general relationships[19]

$$e^{i\theta\hat{I}_z}\hat{I}_+e^{-i\theta\hat{I}_z}=\hat{I}_+e^{i\theta},$$
$$e^{-i\hat{I}_z\theta}\hat{I}_xe^{i\hat{I}_z\theta}=\hat{I}_x\cos\theta+\hat{I}_y\sin\theta,$$
$$e^{-i\hat{I}_y\theta}\hat{I}_xe^{i\hat{I}_y\theta}=\hat{I}_x\cos\theta-\hat{I}_z\sin\theta,$$

one obtains

$$S(t)=\tfrac{1}{2}[\cos\beta\cos(\varphi_0+\gamma)+i\sin(\varphi_0+\gamma)]\times e^{i(\varphi-\varphi_0)}\,\mathrm{Tr}(I_-I_+). \quad \text{(B4)}$$

Upon collecting like terms, one obtains

$$S(t)=\tfrac{1}{3}I(I+1)(2I+1)[Ae^{-i\gamma}+Be^{i\gamma}], \quad \text{(B5)}$$

where $A=-e^{i\Delta\omega(t-2\tau)}\sin^2(\beta/2)$

$$B=e^{i\Delta\omega t}\cos^2(\beta/2).$$

APPENDIX C: FOURIER TRANSFORMS AND MOMENTS

It can be shown in a straightforward manner that the expression

$$S(t)=\exp(-\tfrac{1}{2}a^2t^2)(\sin bt/bt) \quad \text{(C1)}$$

has as its Fourier transform

$$g(\omega)=\frac{1}{2ab\sqrt{2}\pi}\int_{-b}^{b}\exp[-(\omega-\alpha)^2/2a^2]d\alpha, \quad \text{(C2)}$$

where $g(\omega)$ represents the steady-state line-shape function and is equivalent to a superposition of Gaussians under a rectangle of width $2b$. Thus for this line-shape function

$$f(\alpha)=(1/2b) \quad \text{for} \quad -b\leqq\alpha\leqq b.$$

The expression

$$S(t)=\exp(-(a^2t^2/2))(J_1(bt)/bt) \quad \text{(C3)}$$

has as its Fourier transform

$$g(\omega)=\frac{1}{ab}\left(\frac{2}{\pi^3}\right)^{1/2}\int_{-b}^{b}\left[1-\left(\frac{\alpha}{b}\right)^2\right]^{1/2}\times\exp[-(\omega-\alpha)^2/2a^2]d\alpha. \quad \text{(C4)}$$

This line-shape function corresponds to a superposition of Gaussian curves under a semicircular envelope of radius b. Thus

$$f(\alpha)=(2/\pi b)[1-(\alpha/b)^2]^{1/2} \quad \text{for} \quad -b\leq\alpha\leq b.$$

If one defines $T_2=\pi g(0)$, then in the limit $a/b\ll1$ one can write for the function (C2) that $T_2=\pi/2b$ and for the line-shape function (C4) that $T_2=4/2b$. In the same approximation, $a/b\ll1$, the steady-state linewidths measured from the derivative curve are approximately $2b$.

The moments of these curves can be found easily from the coefficients of time in the power-series expansion of $S(t)$.

$$S(t)=[\exp(-a^2t^2/2)](\sin bt)/bt$$
$$=1-\tfrac{1}{2}t^2(a^2+\tfrac{1}{3}b^2)+(t^4/4!)(3a^4+2a^2b^2+\tfrac{1}{5}b^4)+\cdots$$

also

$$S(t)=[\exp(-a^2t^2/2)]J_1(bt)/bt$$
$$=1-\tfrac{1}{2}t^2(a^2+\tfrac{1}{4}b^2)+(t^4/4!)(3a^4+\tfrac{3}{2}a^2b^2+\tfrac{1}{8}b^4)+\cdots.$$

Since in general $S(t)=1-(t^2/2!)M_2+(t^4/4!)M_4+\cdots$ one has $M_2=a^2+b^2/3$ and $M_4=3a^4+2a^2b^2+(b^4/5)$ for the rectangular envelope and also $M_2=a^2+b^2/4$ and $M_4=3a^4+(3a^2b^2/2)+(b^4/8)$ for the circular envelope.

To show that the width of the rectangular distribution is approximately $2b$, one can set the second derivative of $g(\omega)$ equal to zero and solve the resulting transcendental equation

$$(x-1/x+1)=\exp(-2(b^2/a^2)x),$$

where $x=\omega/b$. For $a^2/b^2\leq0.2$ then $x=\pm1$ is a good approximation.

[19] C. P. Slichter, *Principles of Magnetic Resonance* (Harper and Row, New York, 1963), Chap. 2.

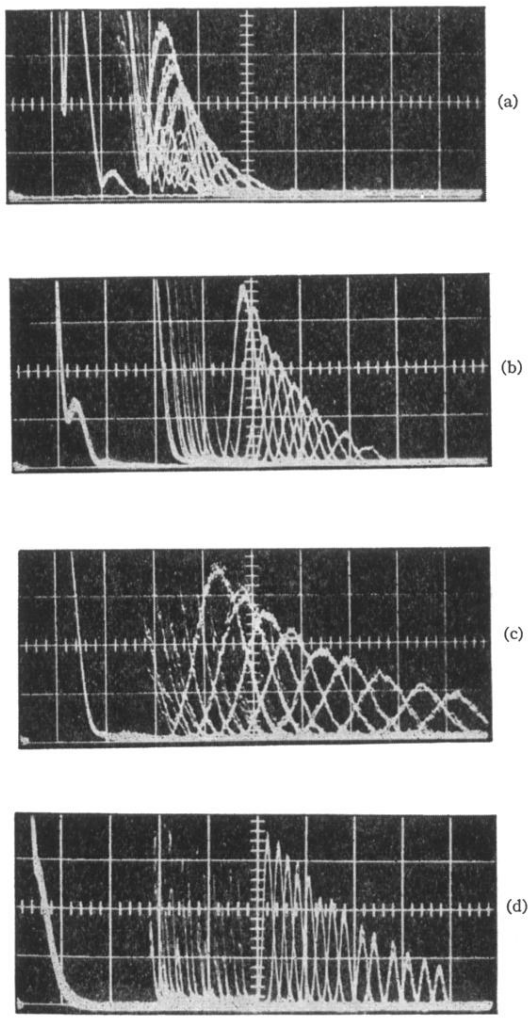

FIG. 10. Echo-decay envelopes at 4.2°K and 1.1°K, $Y=1$ V/division. (a) 75% H_2, $T=4.2$°K, $X=50$ μsec/division. (b) 75% H_2, $T=1.1$°K, $X=50$ μsec/division. (c) 25% H_2, $T=4.2$°K, $X=50$ μsec/division. (d) 25% H_2, $T=1.1$°K, $X=100$ μsec/division.

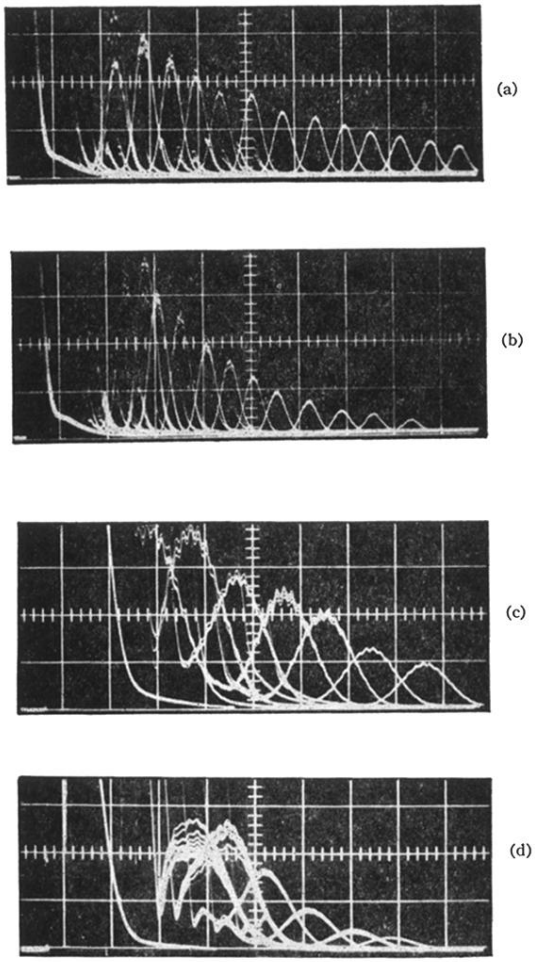

FIG. 11. Echo decays for different values of β at 1.1°K. (a) 25% H_2, $40° < \beta < 60°$, $X = 50$ μsec/division, $Y = 1$ V/division. (b) 25% H_2, $\beta = 90°$, $X = 50$ μsec/division, $Y = 1$ V/division. (c) 75% H_2, $40° < \beta < 60°$, $X = 20$ μsec/division, $Y = 0.5$ V/division. (d) 75% H_2, $\beta = 90°$, $X = 20$ μsec/division, $Y = 1$ V/division.

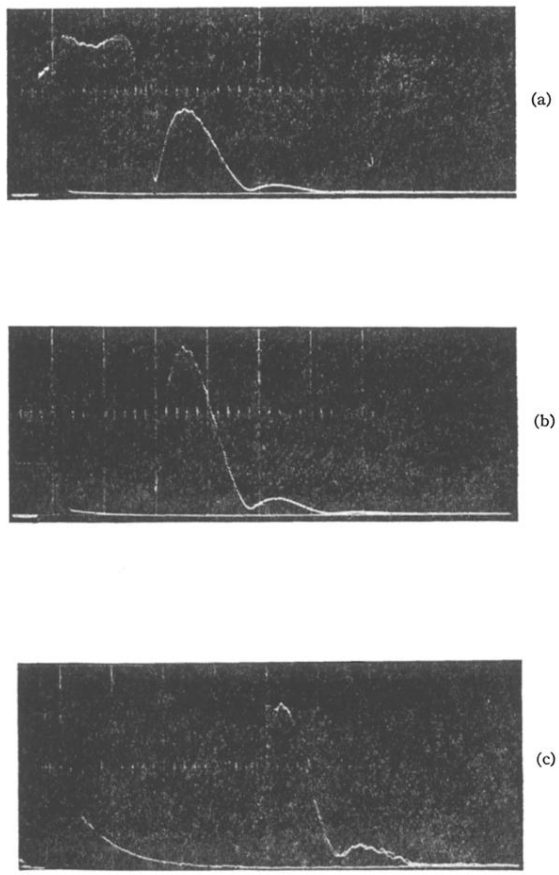

FIG. 2. Bloch decay for nH_2 at 4.2°K, $X=20$ μsec/division. (a) $Y=2$ V/division. (b) $Y=1$ V/division. (c) $Y=0.1$ V/division.

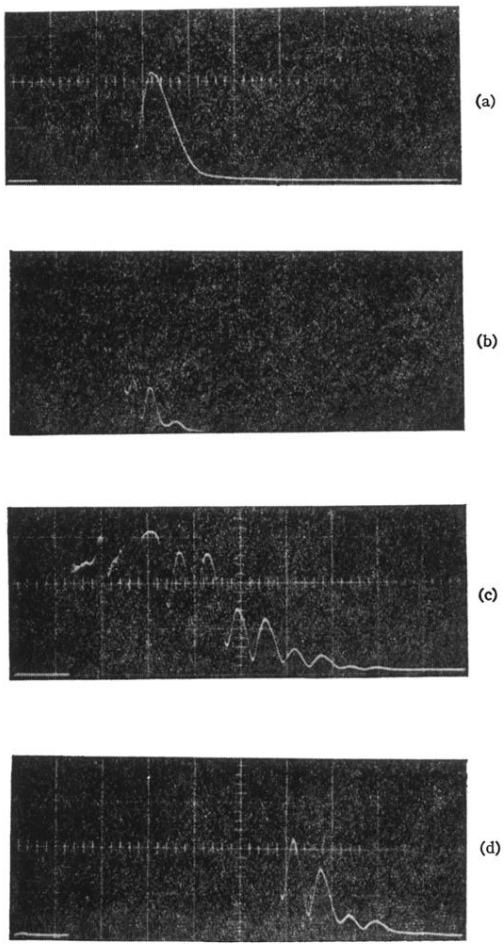

FIG. 3. Bloch decays for nH_2, $1.1°K \leq T < 4.2°K$. (a) $X=20$ μsec/division, $Y=1$ V/division, $T \approx 2°K$. (b) $X=20$ μsec/division, $Y=1$ V/division, $T \approx 1.5°K$. (c) $X=10$ μsec/division, $Y=1$ V/division, $T=1.1°K$. (d) $X=10$ μsec/division, $Y=0.5$ V/division, $T=1.1°K$.

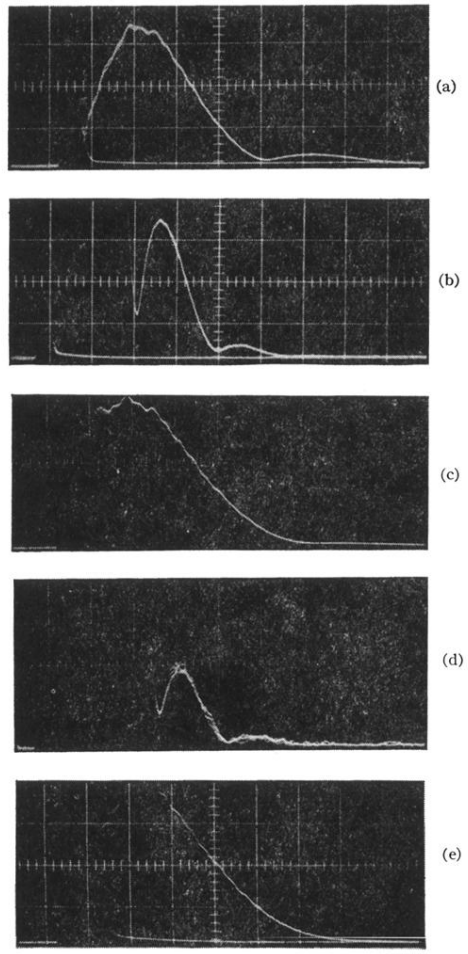

FIG. 4. Bloch decays for mixtures at 4.2°K, $Y=1$ V/division. (a) 75% H_2, $X=10$ μsec/division. (b) 75% H_2, $X=20$ μsec/division, gain$\times$10.4 over (a). (c) 40% H_2, $X=10$ μsec/division. (d) 40% H_2, $X=20$ μsec/division, gain$\times$22.4 over (c). (e) 25% H_2, $X=10$ μsec/division.

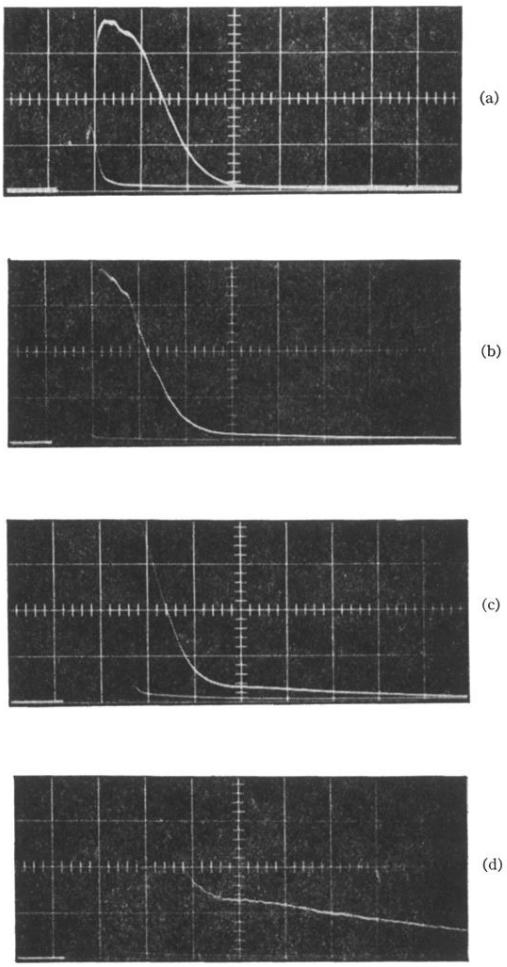

FIG. 5. Low-gain Bloch decays for mixtures at 1.1°K, $X=10$ μsec/division, $Y=1$ V/division. (a) 75% H_2. (b) 40% H_2. (c) 25% H_2. (d) 5% H_2.

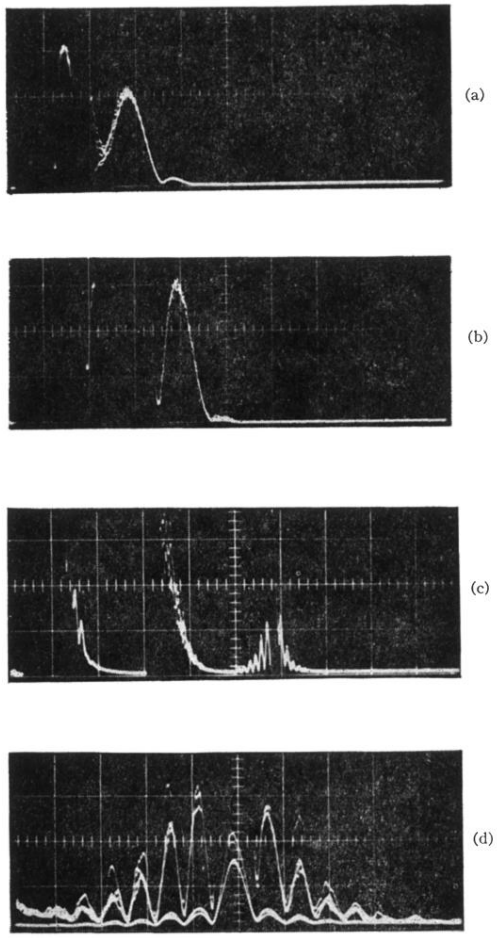

FIG. 7. Spin echoes for nH_2 at 4.2°K and 1.1°K. (a) $T=4.2$°K, $X=50$ μsec/division, $Y=1$ V/division. (b) $T=4.2$°K, $X=50$ μsec/division, $Y=0.1$ V/division. (c) $T=1.1$°K, $X=50$ μsec/division, $Y=0.2$ V/division. (d) $T=1.1$°K, expanded view of an echo (superposition of two photos). $X=10$ μsec/division, $Y=0.5$ V/division and 0.05 V/division.

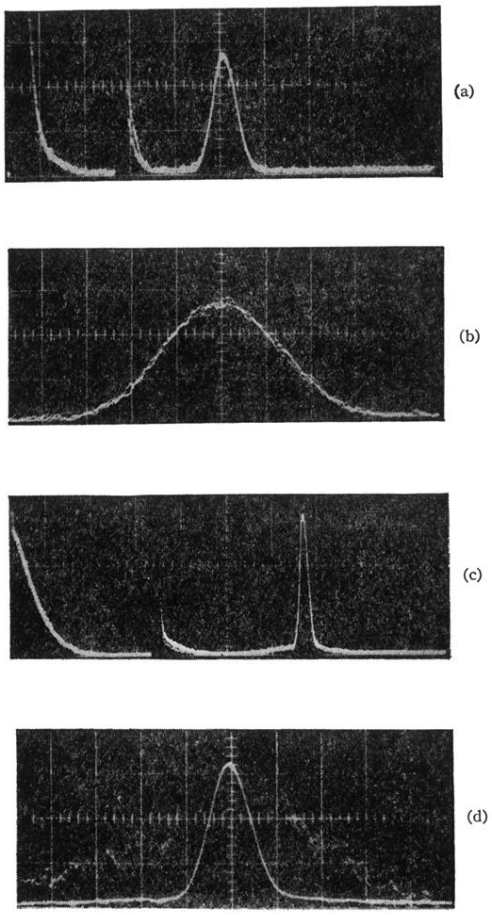

FIG. 8. Spin echoes for 5% mixture at 4.2°K and 1.1°K. (a) $T=4.2$°K, $X=100$ μsec/division, $Y=1$ V/division, $60° < \beta < 90°$. (b) $T=4.2$°K, expanded view of echo, $X=20$ μsec/division. (c) $T=1.1$°K, $X=100$ μsec/division, $Y=1$ V/division, $60° < \beta < 90°$. (d) $T=1.1$°K, expanded view of echo, $X=20$ μsec/division, $Y=1$ V/division.

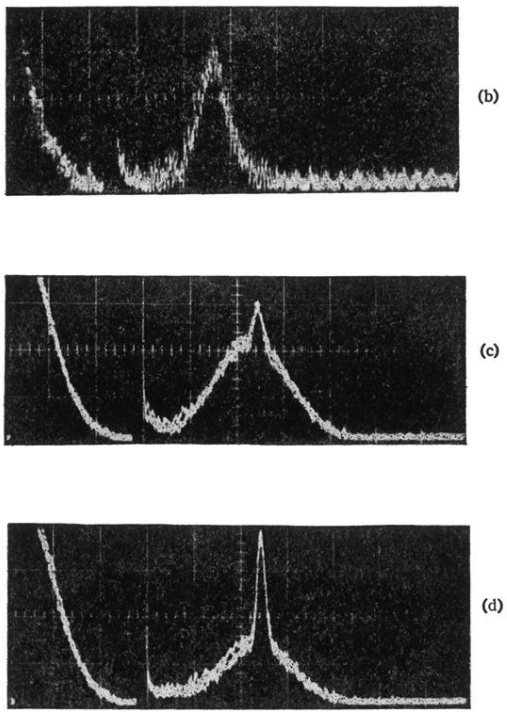

FIG. 9. Spin echoes for 1% mixture at 4.2°K and 1.1°K, $X=100$ μsec/division. (a) $T=4.2$°K, $\beta=180°$, $Y=0.5$ V/division. (b) $T=4.2$°K, $\beta=90°$, $Y=0.5$ V/division. (c) $T=1.1$°K, $\beta=180°$, $Y=1$ V/division. (d) $T=1.1$°K, $\beta=90°$, $Y=1$ V/division.